Journal of Techniques, ISSN: 2708-8383, Vol. 5, No. 4, 2023, Pages 115-130
DOI: https://doi.org/10.51173/jt.v5i4.1278

JOURNAL OF TECHNIQUES

Journal homepage: http://journal.mtu.edu.iq

RESEARCH ARTICLE - ENGINEERING

Experimental Study of the Wickless Heat Pipe Heat Exchanger by Using Nano Fluid

Osamah Raad Skheel[1,2*], Nabil J. Yasin[2], Audai Hussein Al-abbas[3], Sumair Ahmed Soomro[4]

[1]Technical Instructors Training Institute, Middle Technical University, Baghdad, Iraq

[2]Engineering Technical College - Baghdad, Middle Technical University, Baghdad, Iraq

[3]Al-Mussaib Technical College, Al-Furat Al-Awsat Technical University, Kufa, Iraq

[4]Key Laboratory of Advanced Technologies of Materials, Ministry of Education, School of Materials Science and Engineering, Southwest Jiaotong University, Chengdu 610031, China

[*] Corresponding author E-mail: osamah.raad@mtu.edu.iq

Article Info.

Article history:

Received
23 February 2023

Accepted
11 July 2023

Publishing
31 December 2023

Abstract

The use of wickless heat pipe heat exchangers has been improving a wide range of thermal applications such as solar water heaters. Therefore, more scientific research needs to be conducted to improve its performance. In the present study, a wickless heat pipe heat exchanger test rig has been designed and fabricated to investigate the effect of different parameters on its performance. Two different heat pipe working fluids have been used namely pure water and water with nanoparticles (Al_2O_3) using different fluid volume ratios (20%,40%,60%,80%, and 100%). The concentrations of the nanoparticles in water range between 1.3 and 7 % wt. For the heat exchanger, various inlet hot air temperatures (50, 55, and 60 ºC) have been tested at the hot side (heat pipe evaporator) whereas the inlet temperature of the cold side (heat pipe condenser) has been maintained at 20 ºC. The effect of airflow Reynolds number has also been examined with a range of 2583-20664. Results showed that the best heat exchanger effectiveness is achieved at a Reynolds number of 10332 and nanoparticles concentration of 7% wt. Also, the use of nanoparticles reduced the thermal resistance in the heat pipe due to the significant reduction in its surface temperature compared to that of pure water.

Publisher: Middle Technical University

Keywords: Nanofluid; Wickless Heat Pipe; Heat Exchanger; Working Fluid; Effectiveness.

1. Introduction

Wickless heat pipe heat exchanger technology depends on the vaporizing of the used working fluid at the evaporator section due to heat addition, where the outcome vapor is considered as the primer that transports energy from the hot to the cold sides. The vapor movement is executed by the bouncy effect, which is formed in vapor. The condensed drops at the condenser section return to the evaporator zone by the effect of gravity to replay the cycle again. The wickless heat pipe is divided into three main regions and they are evaporator, condenser, and adiabatic sections. Generally, the heat is added at the evaporator and rejected at the condenser meanwhile it passes through the adiabatic section without any loss or addition [1]. It is essential to know that the wickless heat pipe heat exchanger is considered a heat exchanger device, but it transfers the heat energy using a heat pipe and not by the surface contact area such as shell and tube heat exchanger or double tube heat exchanger. From the interesting point of review, the prime mover of the wickless heat pipe heat exchanger can be considered as the used heat pipe this assumption makes us seek more studies that improve the performance of the wickless heat pipe by changing the working fluid type, filling ratios, and heat pipe geometries [2].

The use of refrigeration fluids played an active role in the performance of the thermosiphon; hence Naresh Y. et al 2016 reported experimental results of the internal finned thermosiphon by using water and/or acetone as working fluids. It was conducted A clear effect for the internal finned condenser where the thermal resistance reduction was conducted by 17% and temperature reduction by 35.48% [3]. Also, an obvious enhancement in the thermal performance of the heat pipe was conducted experimentally by M. G. Mousa 2011; where he tended to use AL_2O_3 + water as Nano working fluid so the predictions showed that a reduction in the thermal resistance of the heat pipe was achieved by increasing the concentration of the nanoparticles [4].

Matthias H. et al 2013 carried out experimental investigations for the use of water titanium dioxide and gold Nanoparticles as working fluids in the vertical thermosiphon application. It was found a clear reduction in the thermal resistance (up to 24%) as Nano-fluid was used. Also, it was found increasing of Nano-particle concentration to more than 0.3 vol. % did not provide any further enhancement to the thermal performance of the thermosiphons significantly [5]. A glass thermosiphon charged with acetone and low volume concentration of graphene Nanoparticles was studied by Lazarus G. et al 2015. The achievements conducted a clear reduction in the thermal resistance of thermosiphon

Nomenclature & Symbols			
T	Temperature ^{o}C	FR	Filling Ratio %
EBR	Energy balance Ratio	$T_{c,in}$	Inlet Cold Temperature of Air
L	Length (cm)	ρ	Density ($kg/m^{3)}$
e,eva	Evaporator	ε	Effectiveness
c,con	Condenser	a	Air
a	Adiabatic	h	Hot
Q	Heat Energy (W)	c	Cold
m	Mass Flow Rate (kg/sec)	in	Inlet or Entered
$T_{h,in}$	Inlet Hot Temperature of Air	out	Outlet or Exit

by the increase of Nano-particle concentration by 70.3%. Moreover, the enhancement in the heat transfer coefficient of the evaporator section was achieved in the case of Nanofluid utilization with a rate of 61.25% [6]. Moreover, M.M. Sarafraz et al. 2019 tended to implement the thermosiphon thermal performance using Nano-particles in addition to the working fluid. The conduct enhances the range of heat transfer rate. The best thermal performance of the thermosiphon was obtained when the tilted angle with 60o and a filling ratio of 65% when the zirconia-acetone Nano fluid was used as working fluids [7]. Moreover, Fulpagare et al. 2022 examined the enhancement in the heat transfer rate of thermosiphon when the graphene Nano-particles were mixed with dielectric fluid (HFE-7000) as a working fluid with a concentration of 0.5% wt. The achievements gave more reduction in the thermal resistance by the increase of the input power. Also, the best filling ratio of the used Nano-fluid was notified at 70% when the input heat load was 90 W [8]. Meanwhile, Marine Narcy et al. 2018 performed an experimental study about the thermosiphon that was assisted by a heat spreader plate. The tests included a clear visualization of the effect of water boiling. It was concluded that the orientation angle of the thermosiphon provided a low sensitivity change in the thermal performance [9]. Furthermore, Samuel L. Abreu and Sergio C. 2003 experimentally executed an investigation about heat pipes with different evaporator lengths. It was found throughout the denoted study that thermal resistance was reduced significantly in the case of lower evaporator length [10]. Furthermore, H.M.S Hussein et al 2006 achieved this by experimenting with the use of wickless heat pipes under different geometries. It was achieved that the elliptical shape presented the best performance of the heat pipe. Furthermore, the circular crisscross-section provided a closed thermal performance to the elliptical one, and it is more than that of a semi-circular shape [11]. Meanwhile, K. Ochsner 2008 presented an experimental study about the carbon dioxide usage in fluid in the thermosiphon with different tubes. It was found that the reduction of tube diameter enhances the rate of heat transfer due to an increase in the flow rate [12].

The literature review has a small number of research regarding the experimental study of the wickless heat pipe-heat exchanger. The present study aims to provide a good understanding of the performance of wickless heat pipes under different parameters. The main objective of this study was to experimentally perform the effect of several important parameters such as effectiveness, thermal resistance, filling ratio, and nanoparticles with a wide range of Re numbers. The wickless heat pipe heat exchanger is designed and tested using two different working fluids and with different volume fluid ratios. The energy balance ratio (EBR) and mean surface temperature are also considered and investigated for the wickless heat pipe in the present study. Different concentrations of Al_2O_3 as nanoparticles are implemented with a range of filling ratios to investigate their effects on mean surface temperatures and thermal resistance.

2. Methodology

The present work includes designing, manufacturing, and operating a test rig with the assistance of measurement devices to examine the thermal performance of the wickless heat pipe heat exchanger. Two air ducts are fabricated in such a way that the wickless heat pipe is arranged vertically where the upper duct directs the cold air, meanwhile the lower duct directs the hot air. Every duct is manufactured to form a square cross-section with dimensions of 21×21 cm to get the best hydraulic effect, depending on the unity aspect ratio [13]. Moreover, the duct length is characterized with 320 cm to confirm the effect of fully developed flow for both hot and cold air streams as it was shown in Figs.1 and 2, respectively. It is essential to recognize that the extension of the evaporator and condenser surface area tends to enhance the heat transfer rate between the denoted surfaces and the airflow. Therefore, fins are modified with certain designs and distribution depending on previous scientific outcomes where these fins are shown in the Fig. 3 series [14, 15].

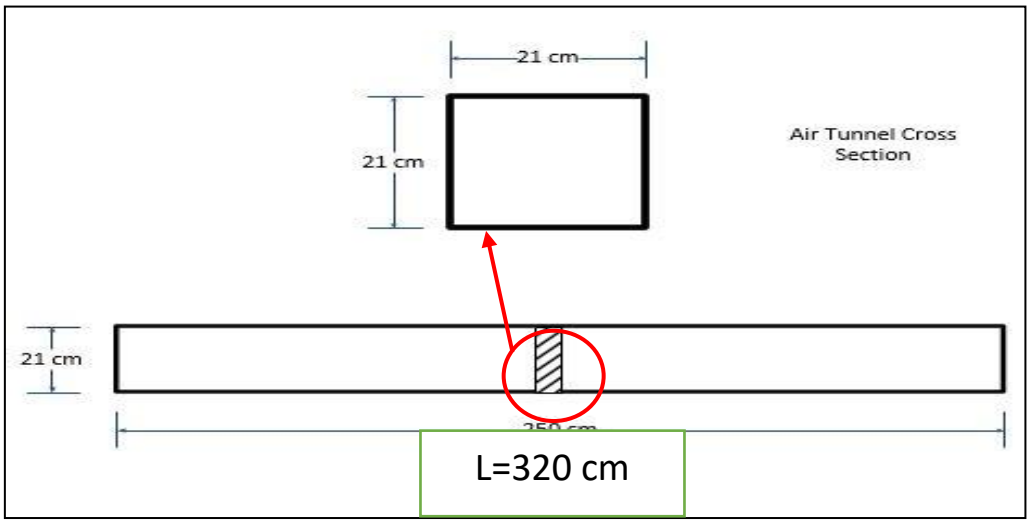

Fig. 1. Schematic diagram of duct

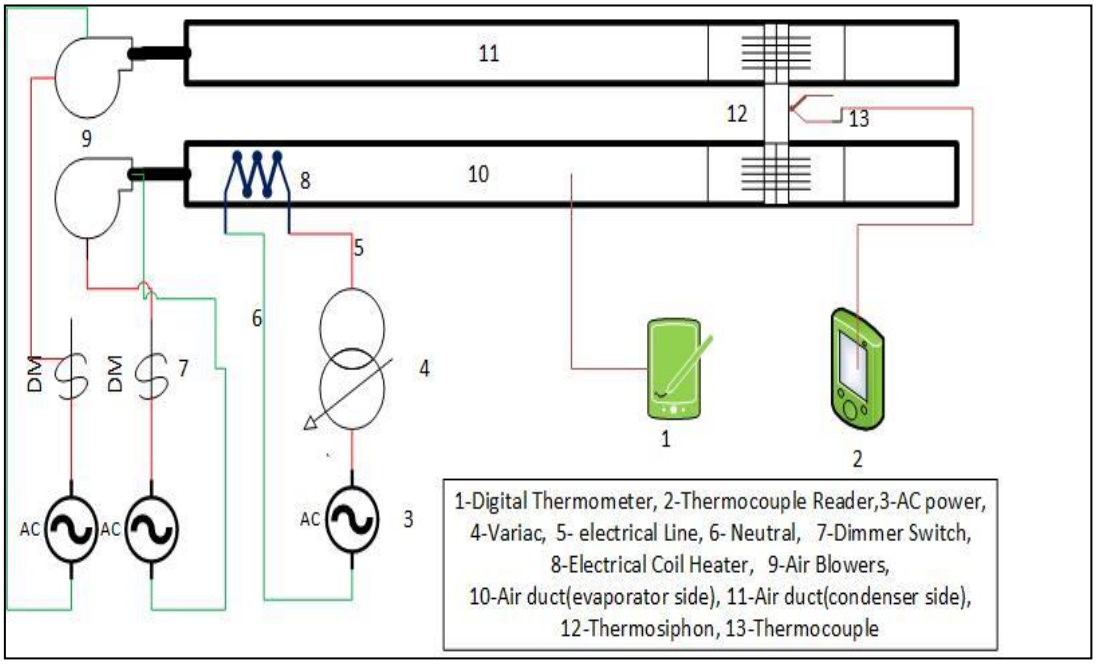

Fig. 2. Schematic diagram of the used test rig

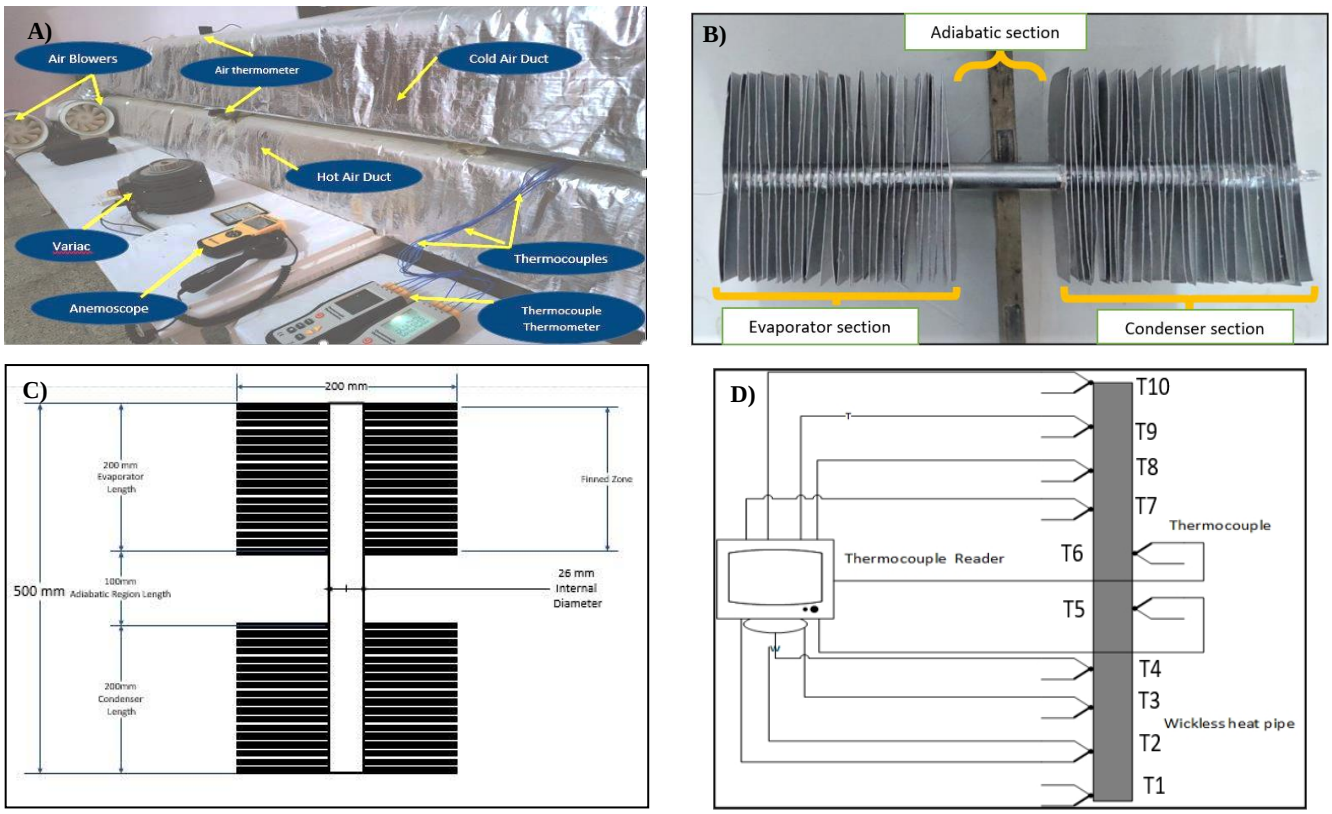

Fig. 3. A) The photograph of the test rig, B) The used wickless heat pipe, C) Dimensions of the wickless heat pipe, D) Thermocouple distribution on wickless heat pipe length

2.1. Experimental procedure setup

- Switching on the axial blowers of the lower and upper ducts.
- Changing the dimmer switch to specify the required airflow speed depending on the anemometer.
- Switching on the electrical heater and specifying the required air temperature of the lower duct by depending on the variac and the readings of the thermometers after the heater.
- Regarding to upper duct i.e. the condenser part of the heat pipe where the lab. The room air conditioning system was controlled to be fixed at 20ºC.

- Noticing the thermometers readings after the evaporator and condenser sections where the dependent readings will be taken after stopping the fluctuating of the thermometer.

The manufactured test rig is formed in such a way that makes the evaporator section or the hot air duct location at the lower level mean while the condenser section is located at the upper level i.e. the cold air duct. This design is necessary to satisfy the thermosiphon operation principle of the wickless heat pipe where the working fluid is still located at the lower part of the pipe when the pipe is settled vertically. Therefore, the hot air duct acts on vaporizing the available working fluid and consequently, the generated vapor goes up to the condenser region using a bouncy effect. The cold air at the condenser section reduces the condenser walls temperature so that the arrived vapor tends to be condensed where newly developed liquid drops on the entire surface of the condenser go down using the gravity effect.

2.2. Measurement devices

2.2.1. Digital thermometer

It is a J-type thermometer that is used to measure the temperature variation throughout any fluid medium, where it has a prop at the end to sense the temperature at the fluid location. The main principle of thermometer depends on converting the temperature value into a voltage signal which should be translated to a digital signal on the LCD screen of the instrument as shown in Fig. 4. This tool is usually used to measure the temperature of the air before and after the evaporator and condenser zones. Moreover, five thermometers are distributed before and after the wickless heat pipe to measure the temperature of the air. Each five thermometer props is arranged according to the form in Fig. 5 to predict all temperature variations in the air streams.

Fig. 4. Digital thermometer with probe

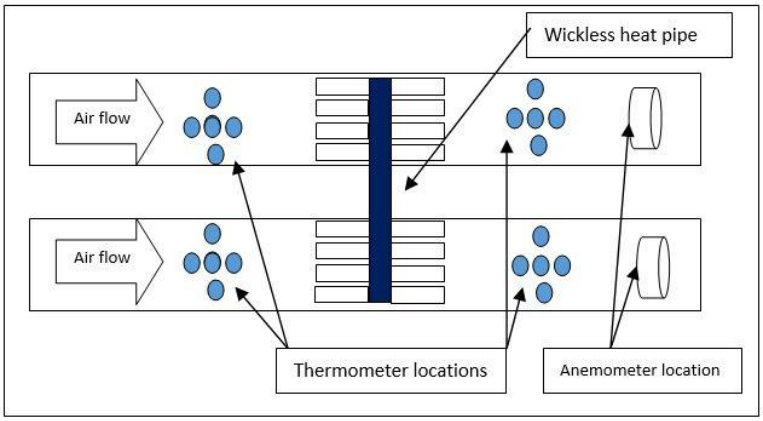

Fig. 5. The distribution of the thermometer props in the cross-section of the duct

2.2.2. Anemometer

It is an aero-electrical instrument used to convert the airflow speed into voltage signals and then transfer it to a digital signal on the LCD screen. This instrument uses a propeller fan that is fixed inside the cylindrical bath, as explained in Fig. 6. Furthermore, the arrangement of the anemometer devices was selected after the heat pipe locations as it was shown in Figs. 4-9.

Then, the airflow is passing to activate the propeller rotation with a certain rotation. This rotation develops a voltage signal that should be transferred by a wired connection to the analysis unit which is used to translate the arrived signal into a reading digital one where the technical specifications of the anemometer have been mentioned in Table 1.

2.2.3. Data Logger

It is an instrument that translates the voltage signals of the K-type thermocouples into temperature readings and displays them on the LCD screen as shown in Fig. 7.

Fig. 6. Anemometer of the test rig

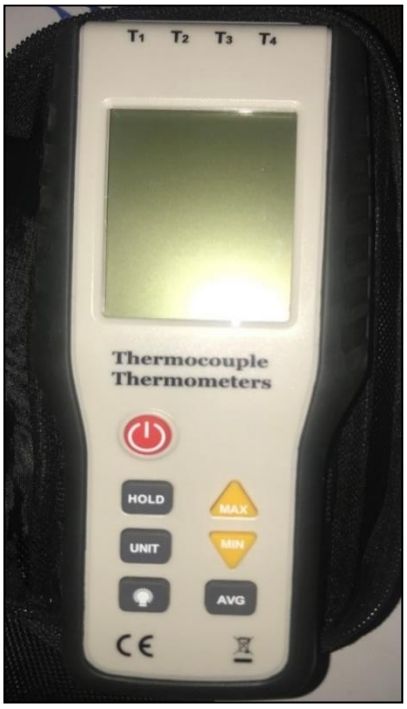

Fig. 7. Data logger

Fig. 8. Axial flow blower

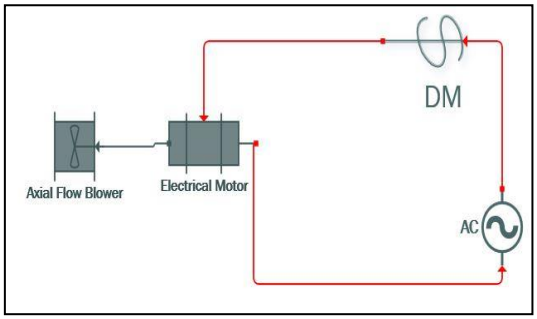

Fig. 9. Dimmer switch electrical connection

Table 1. Anemometer specifications

No	Item	Range
1	Title Name	Hold Peak HP 826-A
2	Air Speed Range	0 ~ 30 m/s
3	Air Temperature range	-10 ~ 60 ºC
4	Powered by	Battery 9 V
5	Accuracy	± 5 %

2.3. Accessories devices

2.3.1. Axial flow blowers

This device which is shown in Fig. 8 is used to provide the suitable quantity of air flow rate under the ranges of the study tests. The axial flow blower was joined with a dimmer switch electrically to control the RPM of the motor, and then specify the air flow rate. The dimmer switch controls the frequency of the arrived electrical current only. The used blower specification and the dimmer switch are listed in Table 2.

Table 2. Axial flow blower specifications

No.	Item	Range
1	Title Name	AS SKY PIPE FAN HZ-200
2	Voltage	220 V
3	RPM	2500 RPM
4	Frequency	50 Hz
5	Power	130W
6	Capacity	1200 m^3/hr

To control the axial blower motor a dimmer switch was used in a wide range of domestic applications such as controlling the ceiling fan speed and exhaust fan. The principle of operation depends on reducing the in-line current frequency of the source. And then tends to eliminate the cycle of the alternative voltage. From the experience point of view, the used devices in the blowers are electrical motors; therefore, the RPM tends to be controlled. The main connection diagram of the dimmer switch with the electrical motor is shown in Fig. 9.

2.3.2. Variable transformer (Variac)

It is a changeable coil transformer that is used to reduce or increase the voltage for any suitable purpose. This device is essentially used to control the electrical heater to control the entering air temperature into the evaporator section. The technical specification of the variance is explained in Table 3.

Table 3. Variac specifications

No.	Item	Range
1	Name Title	VDE 0552
2	Manufacture	Germany
3	Voltage	0 ~ 250 V
4	Frequency	50 Hz
5	Current	10 Amb

2.3.3. vacuum pump

It is a double-stage reciprocated pump that is used to evacuate the closed container from any gases and make the pressure inside it reach -101.325 kpa. This machine includes two lines. The first one is the vacuum line that connects to any container to make it fully evacuated, while the second one is used to pressurize the container with positive pressure. The second line is useful because it is used to compress the refrigerants with high active pressure inside containers. For that reason, the second line should be characterized with high pressure to be liquefied. The used pump in this study has the following technical specifications, which are listed in Table 4 also shown in Fig. 10.

Table 4. Vacuum pump specifications

No	Item	Range
1	Model	Tst-245
2	Capacity	128 L/min
3	Voltage	220 V, 50Hz
4	Power	0.5 Hp
5	Manufacturer	Spain

Fig. 10. Vacuum pump

2.3.4. Electrical heater coil

A high-power electrical heater coil with 5kw was used to warm up the air in the duct to the specified temperature with the aid of the variac system. This part was located at the beginning of the evaporator section duct to warm the air before it reached the evaporator section of the heat pipe. this tool was coiled in a circular form as it is shown in Fig 11.

Fig. 11. Electrical heater

2.4. Charging process

To charge the working fluid into the evaporator section of the wickless heat pipe; a liquid status must be activated in the evaporator section after ending the process. It should be noted that the active pressure inside the wickless heat pipe must be suitable to achieve the boiling and condensation processes, which depend mainly on the temperature of the hot and cold air in the air ducts. The charging methods of the distilled water and ethanol were carried out by the following steps:

- Specifying the required quantity of the distilled water that reaches the required filling ratio.
- Use a picker tool to specify the required amount of the working fluid i.e. distillate water or ethanol.
- After charging the required quantity inside the wickless heat pipe. So, it is desired to reduce the active pressure inside the whole heat pipe up to a certain level where evaporation and condensation can be conducted.
- The pressure reduction is done by using a two-stage vacuum pump and Burdon gage.
- It is desired to attain the referred pressure values in Table 5 to satisfy the liquid phase inside the thermosiphon before the operation.

Table 5. Thermophysical properties of the used working fluids

Working fluid	Thermosiphon-charged pressure kpa	Saturated temperature ºC	Enthalpy of vaporization kJ/kg	Conductivity w/m.K
Ethanol	25	46.6	891.9	0.163
Water	10	45.82	2386	0.625

Regarding the R-1234yf charging process, there are some difficulties during the charging process because that is a gas under room temperature while the prime condition makes it liquid at the evaporator section. Also, the thermophysical properties of the R-1234yf are discussed below in Table 6. The charging process includes the following steps and is explained schematically in Fig. 12.

- Locate the wickless heat pipe on the electronic balance and fit all the connections of high-pressure hoses.
- Joining the refrigerant bottle with the vacuum pump the last one has a suction line for the vacuum process and a discharge line that can be used to compress the gases.
- The vacuum pump acts on sucking the R-1234yf in the suction line and then compressing it inside the wickless heat pipe.
- The change in the weight of the electronic balance refers to a new mass compressed inside the wickless heat pipe.

Table 6. Thermophysical properties of the used working fluids

Working fluid	Thermosiphon-charged pressure kpa	Saturated temperature ºC	Enthalpy of vaporization kJ/kg	Conductivity w/m.K
R1234-yf	1200	46.62	123.4	0.055

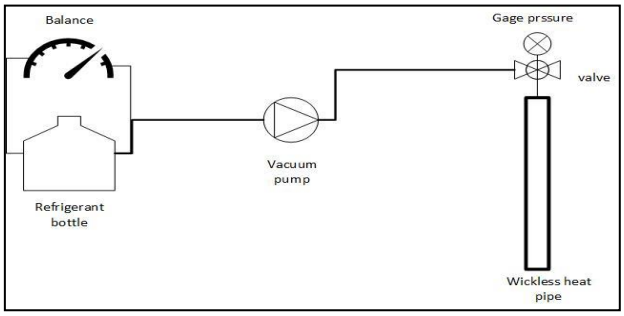

Fig. 12. Refrigerant charging diagram

2.5. Uncertainty and error analysis

Any experimental work is affected by the accuracy of the measurement devices and the response time of extracting the results. Therefore, multi-computation procedures should be followed to check the generated errors during tests. Kline and McClintock method was used to predict those values of uncertainty [16]. This method depends on the governed equation of each discussed parameter, where the equation of mass flow rate depends on mass density, area of flow, and the velocity of flow inside the duct. That, the error deviation of each parameter in the mass flow rate equation should be known then it should be processed by the mathematical relation below to get on the uncertainty of the mass flow rate item.

$$U = R.S$$

$$\frac{\partial U}{U} = \sqrt{\left(\frac{\partial R}{R}\right)^2 + \left(\frac{\partial S}{S}\right)^2}$$

The main measured parameters in the experimental study are hydraulic diameter, air velocity, atmospheric pressure, air temperature, and surface temperature. Therefore, according to the Kline and McClintock method where measured parameters maximum values and uncertainty of the used instruments and the measured parameters should be known as shown in Tables 7 and 8 respectively.

Table 7. The uncertainty of the used instrument

Instrument	Uncertainty
Thermocouple thermometer	±0.1 C
Anemometer	±0.05 m/s
Power meter	±0.01 W
Vernier Clipper	± 1mm
Portable Barometer	± 1.5 kpa
Bordon Gage	± 3.4 kpa
Thermometer	±0.3 C

Table 8. The values of the measured parameters

Parameter	Value
Duct Length	3000 mm
Hydraulic Diameter	210mm
Atmospheric Pressure	110kpa
Maximum applied heat load	2000 W
Ambient Temperature	20 C
Maximum surface temperature	50 C
Maximum air velocity	2 m/s

- Uncertainty of the area cross-section of the airflow (A=I.w): I=w=210mm

$$\frac{\partial \mathrm{A}}{\mathrm{A}} = \sqrt{\left(\frac{\partial \mathrm{I}}{\mathrm{l}}\right)^2 + \left(\frac{\partial \mathrm{w}}{\mathrm{w}}\right)^2} = \sqrt{\left(\frac{1}{210}\right)^2 + \left(\frac{1}{210}\right)^2} = 0.0067$$

- Uncertainty of the duct cross-section perimeter (P=(I+w)*2)

$$\frac{\partial \mathrm{P}}{\mathrm{P}} = \sqrt{\left(\frac{\partial \mathrm{I}}{\mathrm{l}}\right)^2 + \left(\frac{\partial \mathrm{w}}{\mathrm{w}}\right)^2} = \sqrt{\left(\frac{1}{210}\right)^2 + \left(\frac{1}{210}\right)^2} = 0.0067$$

- Uncertainty of the hydraulic diameter ($D_h=\frac{4A}{P}$)

$$\frac{\partial \mathrm{Dh}}{\mathrm{Dh}} = \sqrt{\left(\frac{\partial \mathrm{A}}{\mathrm{A}}\right)^2 + \left(\frac{\partial \mathrm{P}}{\mathrm{P}}\right)^2} = \sqrt{\left(\frac{0.0067}{44100}\right)^2 + \left(\frac{0.0067}{840}\right)^2} = 8 * 10^{-6}$$

- Uncertainty of air density ($\rho = \frac{\mathrm{p}}{\mathrm{RT}}$) : R=0.287kj/kg.K , p=101.325kpa= barometric pressure, $T=T_{ambient}$= 293K=20C

$$\frac{\partial \rho}{\rho} = \sqrt{\left(\frac{\partial \mathrm{p}}{\mathrm{p}}\right)^2 + \left(\frac{\partial \mathrm{T}}{\mathrm{T}}\right)^2} = \sqrt{\left(\frac{1.5}{101.325}\right)^2 + \left(\frac{0.3}{20}\right)^2} = 0.021$$

- Uncertainty of thermal conductivity of air $k=0.0257 * \left(T_f/293\right)^{0.86}$

$$\frac{\partial \mathrm{k}}{\mathrm{k}} = \sqrt{\left(\frac{\partial \mathrm{Tf}}{\mathrm{Tf}}\right)^2} = \sqrt{\left(\frac{0.1}{32.8}\right)^2} = 0.0033$$

- Uncertainty of air velocity inside the air tunnel duct

$$\frac{\partial \mathrm{V}}{\mathrm{V}} = \sqrt{\left(\frac{\partial \mathrm{V}}{\mathrm{V}}\right)^2} = \sqrt{\left(\frac{0.05}{}\right)^2} = 0.0083$$

- Uncertainty of the Reynolds number inside the duct

$$\frac{\partial \mathrm{Re}}{\mathrm{Re}} = \sqrt{\left(\frac{\partial \rho}{\rho}\right)^2 + \left(\frac{\partial \mathrm{V}}{\mathrm{V}}\right)^2 + \left(\frac{\partial \mathrm{Dh}}{\mathrm{Dh}}\right)^2 + \left(\frac{\partial \mu}{\mu}\right)^2}$$

$$\frac{\partial Re}{\mathrm{Re}} = \sqrt{(0.013)^2 + (0.003)^2 + \left(\frac{1}{230}\right)^2 + (0.0033)^2}$$

$$= 0.066$$

- Uncertainty of the dynamic viscosity of the air μ

$$\frac{\partial \mu}{\mu} = \sqrt{\left(\frac{\partial \mathrm{Tf}}{\mathrm{Tf}}\right)^2} = \sqrt{\left(\frac{0.1}{32.8}\right)^2} = 0.0033$$

- Uncertainty of the air mass flowrate

$$\frac{\partial \mathrm{m}}{\mathrm{m}} = \sqrt{\left(\frac{\partial \rho}{\rho}\right)^2 + \left(\frac{\partial \mathrm{V}}{\mathrm{V}}\right)^2 + \left(\frac{\partial \mathrm{A}}{\mathrm{A}}\right)^2}$$

$$\frac{\partial \mathrm{m}}{\mathrm{m}} = \sqrt{\left(\frac{0.021}{1.23}\right)^2 + \left(\frac{0.05}{6}\right)^2 + \left(\frac{0.0067}{0.0441}\right)^2} = 0.15$$

- Uncertainty of the heat exchanger effectiveness

$\frac{\partial\, \varepsilon_S}{\varepsilon_S} = \sqrt{\left(\frac{\partial \mathrm{T}}{\mathrm{T}}\right)^2} = \sqrt{\left(\frac{0.3}{50}\right)^2}$ =0.006 where T represents the inlet and outlet air temperature to the heat exchanger

- Uncertainty of the evaporator and condenser heat energy

$$\frac{\partial \mathrm{Q}}{\mathrm{Q}} = \sqrt{\left(\frac{\partial m}{m}\right)^2 + \left(\frac{\partial \mathrm{T}}{\mathrm{T}}\right)^2}$$

$$\frac{\partial \mathrm{Q}}{\mathrm{Q}} = \sqrt{\left(\frac{0.15}{0.1}\right)^2 + \left(\frac{0.3}{50}\right)^2} = 1.5$$

- Uncertainty of the Energy Balance Ratio EBR

$$\frac{\partial \mathrm{EBR}}{\mathrm{EBR}} = \sqrt{\left(\frac{\partial Q}{Q}\right)^2}$$

$$\frac{\partial \mathrm{EBR}}{\mathrm{EBR}} = \sqrt{\left(\frac{1.5}{400}\right)^2} = 0.00375$$

- Uncertainty of the thermal resistance

$$\frac{\partial \mathrm{Rth}}{\mathrm{Rth}} = \sqrt{\left(\frac{\partial Q}{Q}\right)^2 + \left(\frac{\partial \mathrm{T}}{\mathrm{T}}\right)^2}$$

$\frac{\partial \mathrm{Rth}}{\mathrm{Rth}} = \sqrt{\left(\frac{1.5}{400}\right)^2 + \left(\frac{0.1}{50}\right)^2}$ = 0.00375 where T here represents the surface temperature at the evaporator and condenser section.

3. Data Reduction

To get more accurate results the temperature of the evaporator, adiabatic, and condenser regions are taken as average values among the readings of thermocouples, as shown in mathematical relations below [17].

$$T_e = \frac{T_1 + T_2 + T_3 + T_4}{4} \quad (1)$$

$$T_c = \frac{T_7 + T_8 + T_9 + T_{10}}{4} \quad (2)$$

$$T_a = \frac{T_5 + T_6}{2} \quad (3)$$

The group of T1 to T10 refers to the read temperature by the thermometers that were adopted along the wickless heat pipe as it was shown in the Figure 3 series. Furthermore, the consumed heat energy in the evaporator section or the rejected heat one at the condenser section can be conducted depending on equations 4 and 5 respectively [18].

$$Q_{eva} = cp_a \dot{m}_a \left(T_{out,h} - T_{in,h}\right) \quad (4)$$

$$Q_{con} = cp_a \dot{m}_a (T_{out,c} - T_{in,c}) \quad (5)$$

Effectiveness is the main performance term that tells us how the heat is transferred from the hot side towards the cold one. The effectiveness relation is the ratio between actual heat transfer and the maximum heat transfer therefore it can be written as shown below [19].

$$\varepsilon = \frac{\text{Q actual}}{\text{Q max}} == \frac{m.C.\ (T_{hin} - T_{h,out})}{m.C(T_{h,in} - T_{c,in})} == \frac{T_{hin} - T_{h,out}}{T_{h,in} - T_{c,in}} \quad (6)$$

The energy balance ratio (EBR) is the ratio between the consumed heat energy at the evaporator region and the rejected heat at the condenser region, as shown in the equation below [18]. Moreover, the studied variable parameters that are dependent on the present study are explained in Table 9.

$$EBR = \frac{Q_{eva}}{Q_{con}} \quad (7)$$

Table 9. Variable parameters

No.	Item	Range
1	Inlet hot air temperature (Tin,h)	50, 55, 60° C
2	Inlet cold air temperature (Tin,c)	20 °C
3	Reynolds No. (Re. No.)	2583-20664
4	Filling ratios (FR)	20%,40%,60%,80%,100%
5	Working fluids	Pure water, (AL2O3+Water)

4. Results and Discussion

Fig. 13 conducts the thermal behavior of the heat exchanger concerning different Reynolds number ranges and filling ratios. It is achieved that the maximum value for the effectiveness of the wickless heat pipe heat exchanger has been conducted at the Reynolds number of 10332, meanwhile, an obvious reduction is induced after this value of Reynolds number. The increase of the Reynolds number induces an increase in the air mass flow rate starting from the first Reynolds number value up to the maximum value. So, more heat energy is achieved to be transferred due to the high mass flow rate of the past air. Furthermore, an additional Reynolds number means more air mass flow rate i.e. after the value of Re (10332). That might increase the frictions between the contact surface of the wickless heat pipe and the air stream; Where higher frictions tend to make additive heat on the contact surfaces in the order that builds additive thermal resistance blockage. This blockage prevents the heat transfer from or to heat pipe contact surfaces i.e., evaporator and condenser sections. Thus, it is noted a reduction in the Reynolds number by increasing the Reynolds number after the peak value.

The filling ratio of 60% achieved the best effectiveness value while 100% and 80% are listed in performance after the filling ratio of 60%. This means that the available working fluid in a filling ratio of 60% conducts the best thermal performance for evaporation at the evaporator and condensation at the condenser section of the wickless heat pipe as compared to another filling ratio.

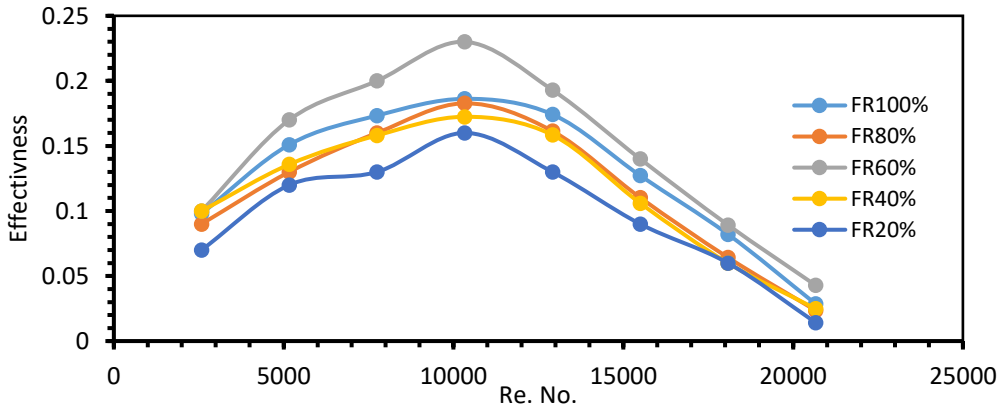

Fig. 13. Wickless heat pipe heat exchanger effectiveness under different Reynolds number and filling ratios and the use of water as working fluid at an inlet temperature of 50°C

Fig. 14 shows the same trend of the effectiveness as function as the Reynolds number but concerning different inlet hot air temperature i.e. hot air stream; Where the lower effectiveness values are formed at inlet hot air temperature of 50° C while the highest ones are at 60° C. The increase of the inlet hot air temperature refers to increasing the heat energy in the hot airstream of the wickless heat exchanger so that, according to the effectiveness relation (eq.6) the heat transfer rate (Q actual) tends to augment the order that enlarges the value of the effectiveness as whole. Physically, the increase of Th, in makes absolutely an augmentation for the Th, out because the heat transfer from the hot air towards the evaporator section of the heat pipe is approached to be fixed due to constant surface area, working fluid type, and geometries. So, Q actual tends to be enhanced due to increasing the Th, in and consequently an augmentation for the Q actual has been reached.

Regarding the energy balance ratio (EBR) performance the best values should be conducted when it reaches unity; so, the unity value of the EBR refers that the consumed heat energy by the wickless heat pipe evaporator is rejected completely by the condenser section of the denoted heat pipe. Fig. 15 shows the experimental results of the EBR concerning the used Re. No. under different filling ratios. It is well explained that an enhancement in the EBR by increasing the Reynolds number starting from the first tested value of Reynolds number up to a range of 10332 where this trend is satisfying the effectiveness performance in Figs. 13 and 14. Also, the filling ratio plays an active role in specifying the best

EBR values as compared to each other where it is noticed that the best EBR values are conducted at filling ratios of 60, 80 and 100% respectively. The increase of the EBR values after the Reynolds number limit i.e. 10332 refers to reducing the heat transfer through wickless heat pipe due to increasing the frictions between air and heat pipe surfaces and enlargement of the thermal resistance.

The effect of the inlet hot air temperature on the behavior of EBR is noticed in Fig. 16; where it is noticed that an obvious reduction in the mean values of EBR by increasing the inlet air temperature. This should be validated because of being the increase in the hot air temperature augments the consumed heat energy by the evaporator so according to equation 7.

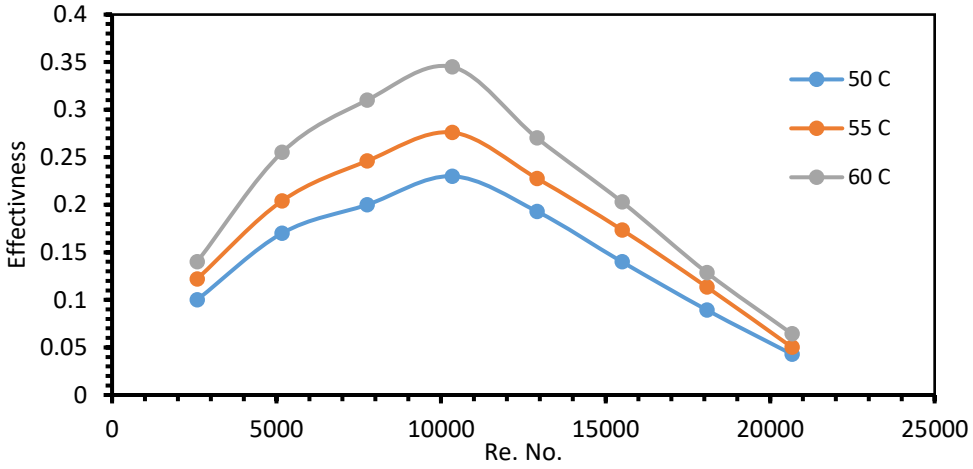

Fig. 14. Wickless heat pipe heat exchanger at different input temperatures of the hot duct and filling ratio of 60% of the water working fluid

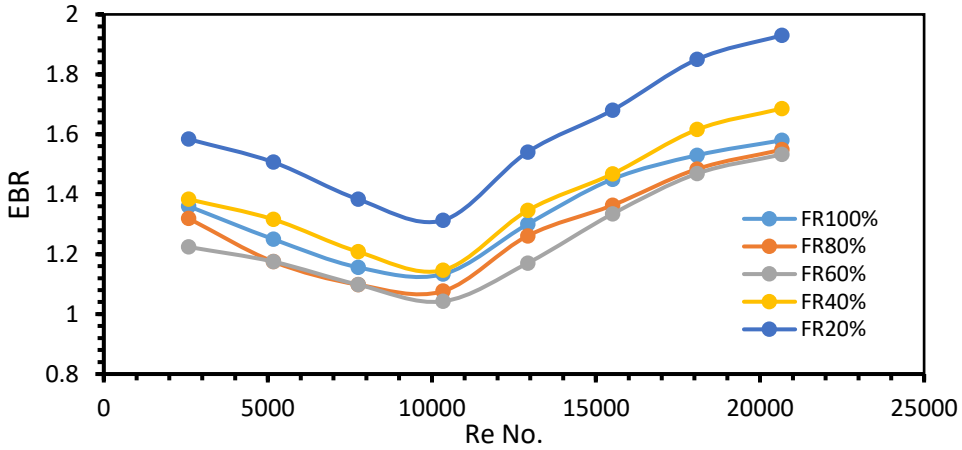

Fig. 15. Wickless heat pipe heat exchanger EBR at different Reynolds numbers at different filling ratio values and using water as working fluid, 50 ºC

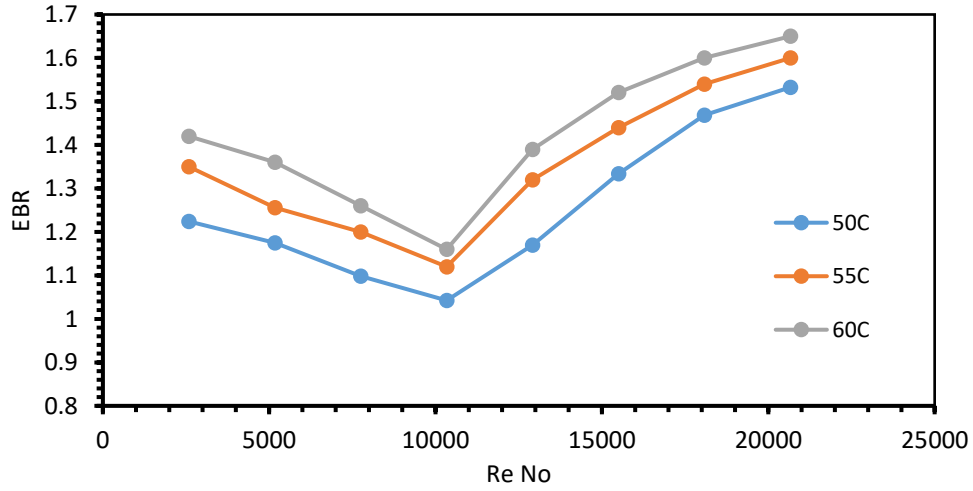

Fig. 16. Effect of EBR under different inlet hot air with FR 60% of water

The thermal resistance of the wickless heat pipe is defined as the ratio between the change in the average temperature of the evaporator and condenser sections to the added heat energy in the heat pipe. The added heat energy can be estimated by calculating the input heat energy to the evaporator section [20]. The thermal resistance parameter is used to predict the total thermal performance of the wickless heat pipe where it can execute a direct effect on the heat exchanger's thermal performance. Regarding Fig.17; where the obvious reduction of thermal resistance values has been obtained up to the Reynolds number value of 10332. This trend satisfied the previous performance parameters such as EBR and effectiveness which present that the best thermal performance can be conducted at Reynolds number of 10332. This is because of increasing the perfection of wickless heat pipe performance i.e. perfect mass flow rate inside the wickless heat pipe the order that reduces the heat accumulations outside of the wickless heat pipe walls.

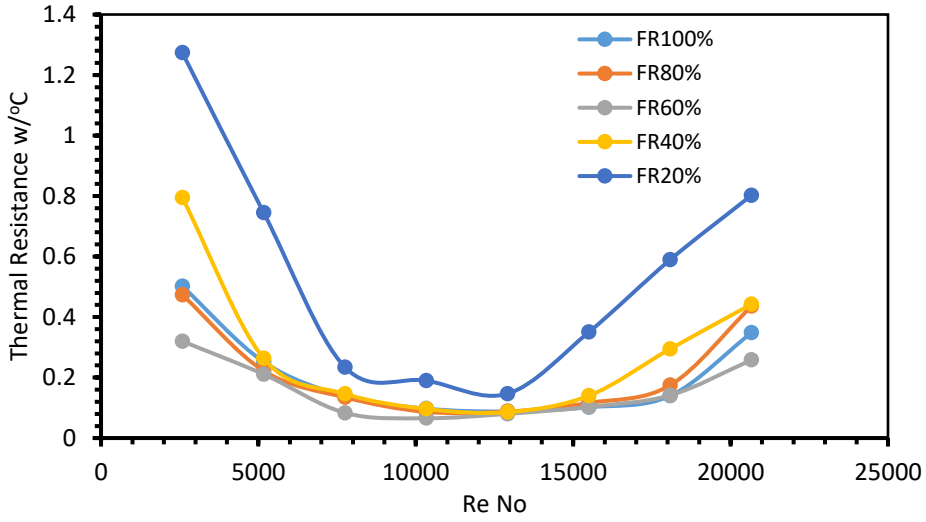

Fig. 17. Thermal resistance of wickless heat pipe with Reynolds number using different filling ratios

It can be extracted that the mean values of thermal resistance have been varied directly with the increase of the inlet hot air temperature because of being that higher temperature degree makes additive heat energy; where this augments the thermal resistance over the external surface of the evaporator section. Consequently, Fig. 18 explained a direct proportion relation between the thermal resistance of wickless heat pipe and the applied Reynolds number under different inlet hot air temperatures.

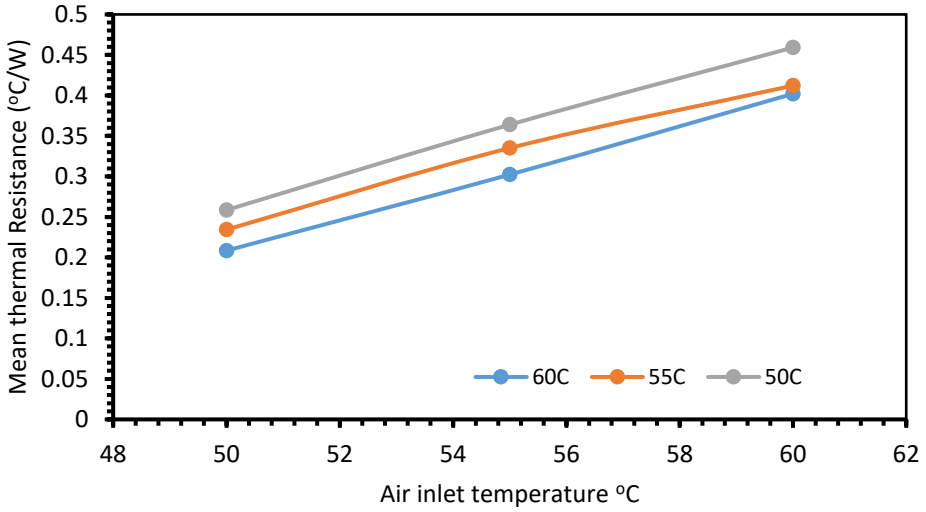

Fig. 18. Effect of inlet air temperature concerning average values thermal resistance at FR100% of water

Regarding the nanofluid utilization, it is well known that these additives are used to improve the overall thermal performance of the wickless heat pipe heat exchanger. The previous analysis tested and discussed the use of water to improve the effectiveness and the EBR of the wickless heat pipe heat exchanger by implementing different filling ratios, Reynolds numbers, and inlet hot air temperatures. Therefore, it is proposed to add Al_2O_3 as Nanoparticles to the water under different percentage weights such as 1%, 3%, and 7%wt respectively.

Figs. 19 and 20 explain the variation in the temperature distribution along wickless heat pipe for the cases of with and without Nano fluid addition. It is obvious that the temperature values are highly achieved for the case of pure distillate water utilization; meanwhile, a reduction in those values is noticed for the case of Nanofluid used. Also, the lower temperature distribution values are shown when there is an increase in the Nanoparticle concentration. This trend is because of being the Nanofluid can transfer more heat energy from the evaporator section to the condenser one as compared to the pure distillate water used. Moreover, the increase in the Nanoparticle concentration tends to increase the effect of the heat transfer process. Consequently, the higher heat transfer rate throughout the heat pipe acts to prevent heat energy accumulation at the heat pipe walls.

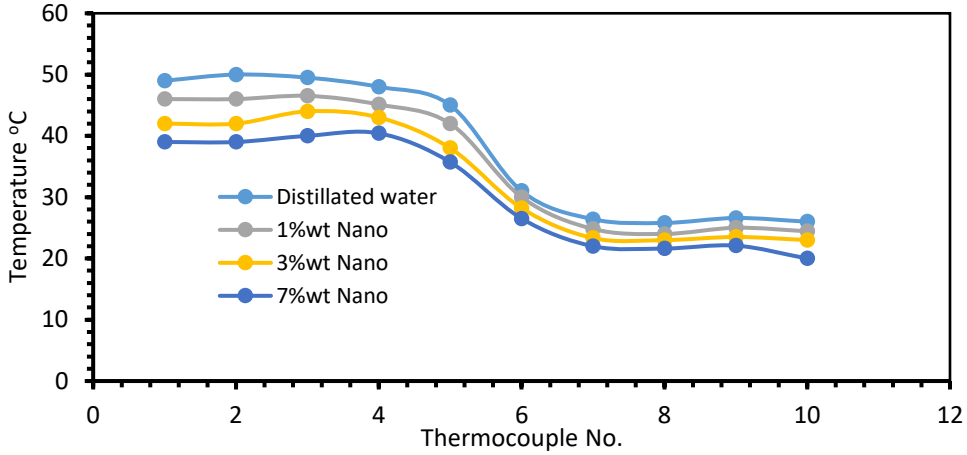

Fig. 19. Effect of nanoparticles concentration of surface temperature of heat pipe at FR100%, Re=10332

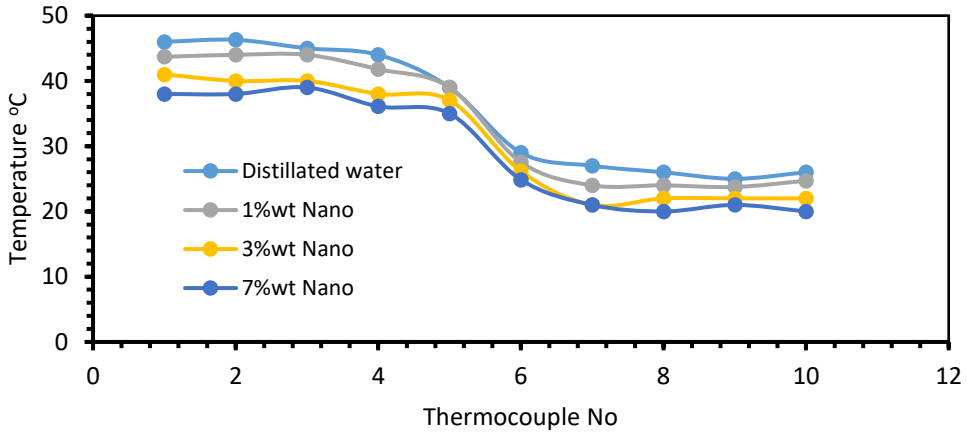

Fig. 20. Effect of nanoparticles concentration of surface temperature of heat pipe at FR60%, Re=10332

Fig. 21 indicates that the increase in the Nanoparticle concentration throughout Nano fluid tends to enhance the heat transfer rate in the wickless heat pipe by eliminating the average surface temperature of the heat pipe. It is conducted that a clear reduction in the mean surface temperature by increasing the Nanofluid concentrations. Moreover, the denoted Fig shows that the increase of the filling ratio acts on increasing the mean surface temperature of the wickless heat pipe. This may be due to increasing the mass of the vapor inside the thermosiphon the order that increases the saturated pressure inside the heat pipe due to fixed volume. Therefore, the saturated temperature goes up to make the wall surface temperature go up too

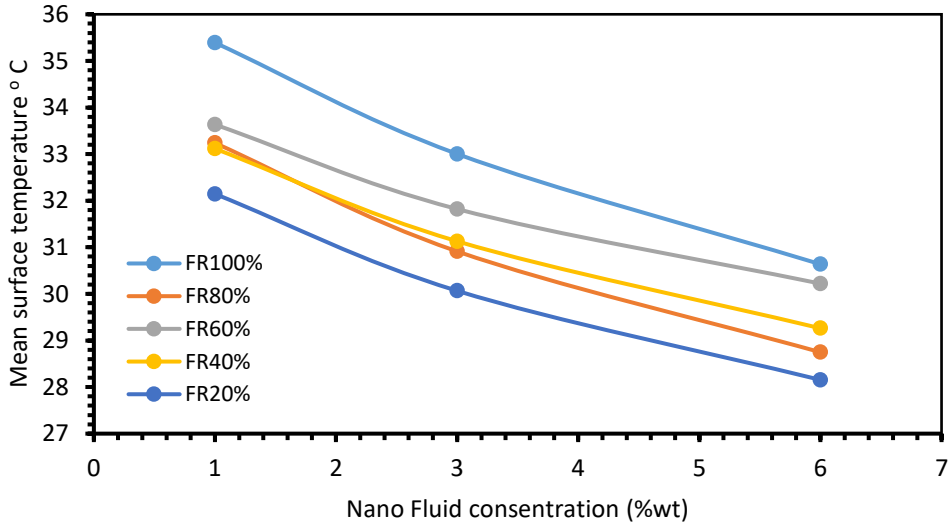

Fig. 21. Effect of nanoparticles concentration on the mean surface temperature of the wickless heat pipe under different filling ratios and Re=10332

Getting a notification for Fig. 22 that implies the effect of thermal resistance of the tested wickless heat pipe by using different concentrations of the Nanoparticles; where it reached a pure reduction in the values of thermal resistance throughout all the range of tested Reynolds number. This reduction is achieved with 10.01%, 14.8%, and 18% for the tested cases of the Nanoparticles concentrations of 1%wt, 3%wt, and 7%wt respectively. This behavior may be due to increasing the thermal conductivity and the enthalpy heat of vaporization of the new Nanofluid.

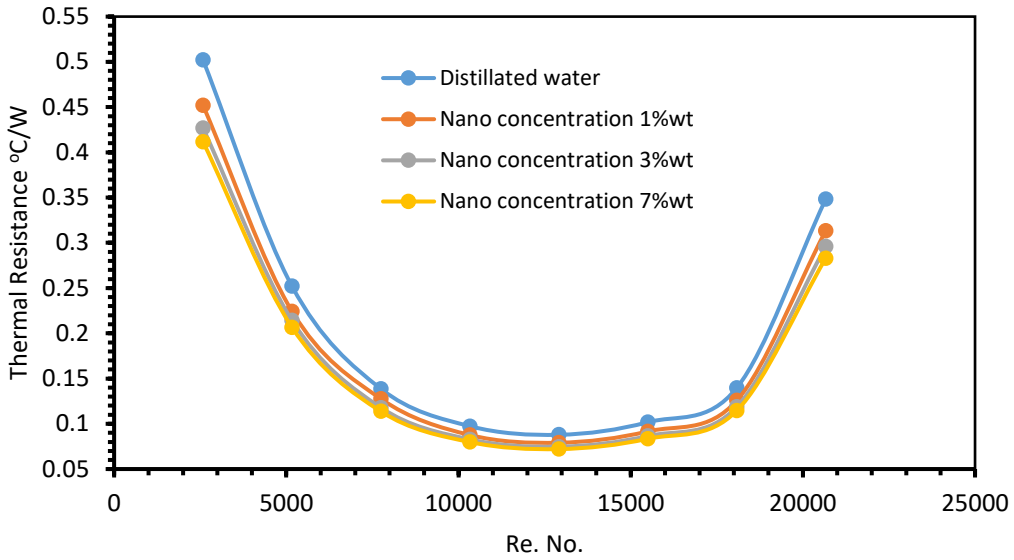

Fig. 22. Effect of thermal resistance of the wickless heat pipe with different nanoparticle concentrations at a hot air temp of 50C

The achieved results are in Fig. 23; so the mean values of thermal resistance of the used wickless heat pipe are dropped down by adding more particles to the used Nanofluid. This may be due to enhancing the thermos-physical properties of the Nano fluid such as thermal conductivity and the enthalpy heat of vaporization where the Nano particles act on transporting more heat energy through the fluid medium. Furthermore, the increase of the mean thermal resistance values is noticed by increasing the inlet hot air temperature which is a result of increasing the heat accumulation at the outer fringes of the heat pipe wall.

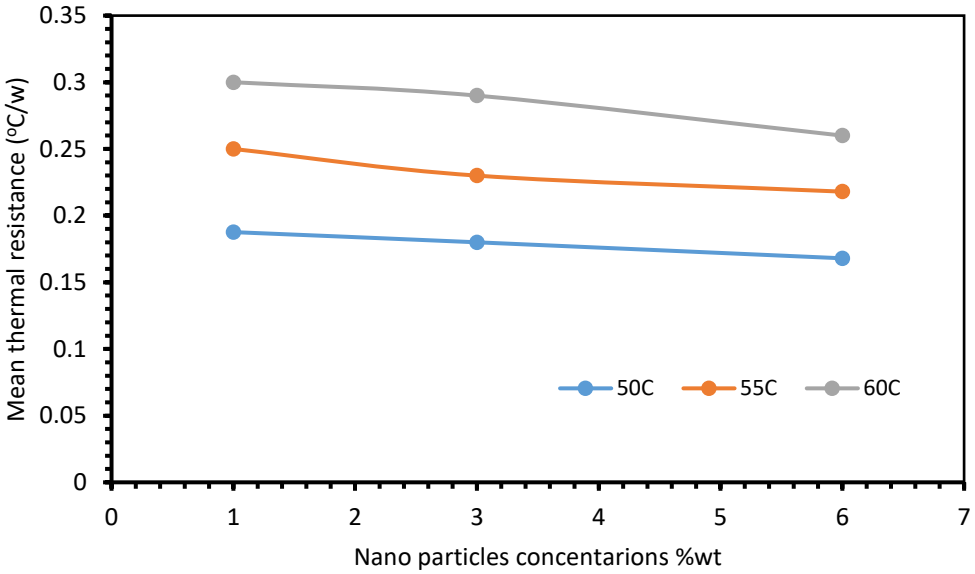

Fig. 23. Effect of nanoparticles concentration on the mean thermal resistance values under different inlet hot air temperature

Referring to Fig. 24, it is noticed that the Nanofluid provides the same trend behavior of the effectiveness where the clear enhancement in the effectiveness values is noticed from the lowest used Reynolds number up to 10332, and then it tends to be reduced up to the highest used Reynolds number. The enhancement may be due to increasing the mass flow rate and reducing the thermal bounded layers over the heat pipe wall. Meanwhile, the reduction is a result of increasing the frictions between the air stream and the fins in the evaporator and condenser regions that tends to increase the thermal bounded layers and consequently eliminate the effectiveness. The effect of Nanoparticle addition supports an increase in the effectiveness with 14%,19%, and 21.2% respectively when the Nanoparticles are 1%et, 3%wt, and 7%wt respectively too. This increase in effectiveness improvement is due to improving the thermos-physical properties of the Nanofluid.

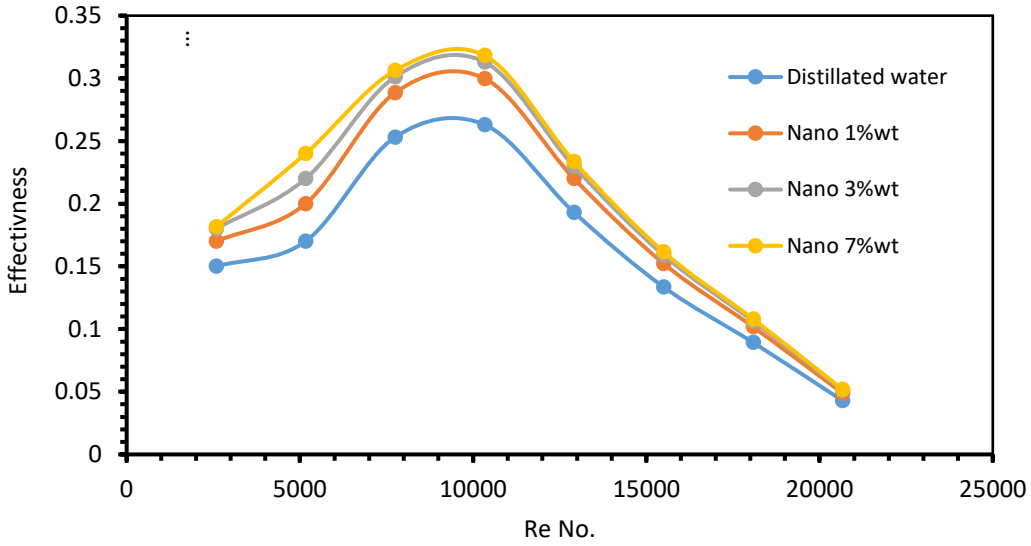

Fig. 24. Effect of the effectiveness values under different Nanoparticle concentrations with FR60%, hot air inlet temperature of 50 ºC

It is essential to know that the nanoparticles tend to enhance the thermos-physical properties of the based fluid (water) where this achievement can be conducted in table 10.

Table 10. Thermal conductivity of the nanofluid at different temperatures

Temperature C	Distilled water K (W/m².K)	Nanofluid 1%wt K (W/m².K)	Nanofluid 3%wt K (W/m².K)	Nanofluid 7%wt K (W/m².K)
30	0.615	0.63	0.69	0.85
45	0.63	0.65	0.73	0.87
60	0.65	0.67	0.75	0.895

5. Conclusions

Thermal performance implementation was carried out on the wickless heat pipe heat exchanger that was filled with pure water and Nanofluid (water+AL_2O_3) under different filling ratios, and Nano particle concentrations, and applied for Reynolds number. The salient conclusions of the present study are:

- The wickless heat pipe has been charged with filling ratios of 20, 40, 60 80, and 100% respectively; where it conducts that 60 % introduces an enhancement in the effectiveness of 34.7% as compared to the worst case i.e. 20% filling ratio.
- The concentration of 7% wt presents the best thermal performance of the whole wickless heat pipe heat exchanger.
- The increase of the nano concentration particles in the based fluid enhances the effectiveness of the wickless heat pipe heat exchanger with rates of 18.7%, 16.12%, and 7.14% for the studied cases of nano additives of 7%wt,3%, and 1% respectively.
- It is found that the operation of a wickless heat pipe heat exchanger under Reynolds number 10332 provides the highest effectiveness values (0.32) and lower thermal resistance (0.8 C/w) as compared to other Reynolds number values.
- The maximum effectiveness value was 0.32 at a filling ratio of 60% and nanoparticle concentration of 7%wt. Meanwhile, the lowest one was 0.265 pure water usage as the working fluid.

Acknowledgment

Great thanks to the credit of the power mechanics department in the technical instructors training institute- Middle Technical University for their valuable role in supplying the measurement instruments.

References

[1] M. Može, A. Nemanič, and P. Poredoš, “Experimental and numerical heat transfer analysis of heat-pipe-based CPU coolers and performance optimization methodology,” Appl Therm Eng, vol. 179, Oct. 2020, doi: 10.1016/j.applthermaleng.2020.115720.
[2] W. Srimuang and P. Amatachaya, “A review of the applications of heat pipe heat exchangers for heat recovery,” Renewable and Sustainable Energy Reviews, vol. 16, no. 6. pp. 4303–4315, Aug. 2012. doi: 10.1016/j.rser.2012.03.030.
[3] Y. Naresh and C. Balaji, “Experimental investigations of heat transfer from an internally finned two phase closed thermosyphon,” Appl Therm Eng, vol. 112, pp. 1658–1666, 2017, doi: 10.1016/j.applthermaleng.2016.10.084.
[4] M. G. Mousa, “Effect of nanofluid concentration on the performance of circular heat pipe,” Ain Shams Engineering Journal, vol. 2, no. 1, pp. 63–69, 2011, doi: 10.1016/j.asej.2011.03.003.
[5] M. H. Buschmann and U. Franzke, “Improvement of thermosyphon performance by employing nanofluid,” International Journal of Refrigeration, vol. 40, pp. 416–428, 2014, doi: 10.1016/j.ijrefrig.2013.11.022.

[6] L. G. Asirvatham, S. Wongwises, and J. Babu, "Heat transfer performance of a glass thermosyphon using graphene-acetone nanofluid," J Heat Transfer, vol. 137, no. 11, pp. 1–9, 2015, doi: 10.1115/1.4030479.
[7] M. M. Sarafraz, O. Pourmehran, B. Yang, and M. Arjomandi, "Assessment of the thermal performance of a thermosyphon heat pipe using zirconia-acetone nanofluids," Renew Energy, vol. 136, pp. 884–895, 2019, doi: 10.1016/j.renene.2019.01.035.
[8] Y. Fulpagare, D. Y. Tsai, and C. C. Wang, "Performance of two-phase loop thermosiphon with graphene nanofluid," Appl Therm Eng, vol. 200, no. October 2021, p. 117714, 2022, doi: 10.1016/j.applthermaleng.2021.117714.
[9] M. Narcy, S. Lips, and V. Sartre, "Experimental investigation of a confined flat two-phase thermosyphon for electronics cooling," Exp Therm Fluid Sci, vol. 96, no. September 2017, pp. 516–529, 2018, doi: 10.1016/j.expthermflusci.2018.01.018.
[10] S. L. Abreu and S. Colle, "An experimental study of two-phase closed thermosyphons for compact solar domestic hot-water systems," Solar Energy, vol. 76, no. 1–3, pp. 141–145, 2004, doi: 10.1016/j.solener.2003.02.001.
[11] H. M. S. Hussein, H. H. El-Ghetany, and S. A. Nada, "Performance of wickless heat pipe flat plate solar collectors having different pipes cross sections geometries and filling ratios," Energy Convers Manag, vol. 47, no. 11–12, pp. 1539–1549, 2006, doi: 10.1016/j.enconman.2005.08.009.
[12] K. Ochsner, "Carbon dioxide heat pipe in conjunction with a ground source heat pump (GSHP)," Appl Therm Eng, vol. 28, no. 16, pp. 2077–2082, 2008, doi: 10.1016/j.applthermaleng.2008.04.023.
[13] A. Bhatia, "HVAC - How to Size and Design Ducts," Continuing Education and Development, Inc., no. 877, p. 89, 2001.
[14] B. Kundu and P. K. Das, "Performance and optimum design analysis of convective fin arrays attached to flat and curved primary surfaces," International Journal of Refrigeration, vol. 32, no. 3, pp. 430–443, 2009, doi: 10.1016/j.ijrefrig.2008.08.012.
[15] X. Yang, J. Guo, B. Yang, H. Cheng, P. Wei, and Y. L. He, "Design of non-uniformly distributed annular fins for a shell-and-tube thermal energy storage unit," Appl Energy, vol. 279, no. July, p. 115772, 2020, doi: 10.1016/j.apenergy.2020.115772.
[16] O. Raad, "The improvement of the solar air heater duct by wired ribs utilization," Karbala International Journal of Modern Science, vol. 5, no. 3, 2019, doi: 10.33640/2405-609X.1163.
[17] A. Ozsoy and R. Yildirim, "Prevention of icing with ground source heat pipe: A theoretical analysis for Turkey's climatic conditions," Cold Reg Sci Technol, vol. 125, pp. 65–71, 2016, doi: 10.1016/j.coldregions.2016.02.003.
[18] S. I. Haider, Y. K. Joshi, and W. Nakayama, "A natural circulation model of the closed loop, two-phase thermosyphon for electronics cooling," J Heat Transfer, vol. 124, no. 5, pp. 881–890, 2002, doi: 10.1115/1.1482404.
[19] Y. A. Çengel, "Heat Exchangers," in Heat Transfer Engineering, 2009, pp. 609–662.
[20] Fadhl, Bandar. Modelling of the thermal behaviour of a two-phase closed thermosyphon. Diss. Brunel University London, 2016, http://bura.brunel.ac.uk/handle/2438/12871.